PHOTONICS Research

# Experimental investigation of ghost imaging of reflective objects with different surface roughness

Suqin Nan, Yanfeng Bai,* Xiaohui Shi, Qian Shen, Lijie Qu, Hengxing Li, and Xiquan Fu

College of Computer Science and Electronic Engineering, Hunan University, Changsha 410082, China
*Corresponding author: yfbai@hnu.edu.cn

Received 24 March 2017; revised 10 June 2017; accepted 27 June 2017; posted 27 June 2017 (Doc. ID 291390); published 26 July 2017

**We present an experimental demonstration of ghost imaging of reflective objects with different surface roughness. The influence of the surface roughness, the transverse size of the test detector, and the reflective angle on the signal-to-noise ratio (SNR) is analyzed by measuring the second-order correlation of the light field based on classical statistical optics. It is shown that the SNR decreases with an increment of the surface roughness and the detector's transverse size or a decrease of the reflective angle. Additionally, the comparative studies between the rough object and the smooth one under the same conditions are also discussed.** 

***OCIS codes:*** (100.0100) Image processing; (110.1650) Coherence imaging; (030.6600) Statistical optics; (030.5770) Roughness.

https://doi.org/10.1364/PRJ.5.000372

## 1. INTRODUCTION

Different from traditional imaging, which detects the signal and records the image of an object using only a detector with high spatial resolution, ghost imaging (GI) is a transverse active-imaging technique that retrieves information from an unknown object by measuring spatial intensity correlation between two light beams. After one beam interacts with the object, the generated scatters are collected by the single-pixel detector or a bucket detector, and the other beam is directly counted by a spatially resolving detector. Since the first experiment was performed using entangled photon pairs produced by spontaneous parametric down-conversion [1,2], the results led to a very lively discussion about whether quantum entanglement is necessary to realize correlated imaging. It was subsequently demonstrated that a pseudothermal source can also be used to implement GI [3–6], which provides more practical applications compared to the entangled source. In recent years, researchers have devoted a good deal of effort to GI with thermal light and some new methods have been reported to improve the imaging quality [7–19], such as pseudo-inverse GI [7,8], compressive sensing GI [9–13], and three-dimensional GI [13–15].

Most GI experiments and related theory refer to the transmissive case. However, in practical application, almost all targets are reflective or diffuse. Thus, compared to GI with a transmission target, reflective GI (RGI) is closer to the demands of practical applications. In 2008, the first reflective experiment was conducted using a toy [20]. Unlike this experiment, the ghost-image reconstruction of a diffuse-reflecting object consisting of two strips allowed researchers to vary the relevant parameters in a wide range and perform numerical simulations [21]. Over the years, the influencing factors of RGI quality have also attracted much concern, and many studies continuously emerged [22–28]. Researchers explored the effects of the transverse dimension and coherence width of the light source on the image quality and found that the higher coherence width contributed to higher visibility but resulted in poor resolution, which was inversely proportional to the transverse dimension of the source [22]. Researchers then theoretically studied the resolution, contrast, and signal-to-noise ratio (SNR) in an RGI system [23]. By using numerical simulations, researchers demonstrated that both the surface height variance and the correlation length, which have been introduced to characterize the rough surface, had no influence on the image resolution [25]. Obviously, the previous studies based on rough objects are almost all theoretical. From previous works [20,21], it was discovered that RGI must detect all the photons reflected from the object surface to reconstruct the ghost image. While it is demonstrated theoretically that the rough object's image can be reconstructed by GI, even using a single point-like detector [28]. In this paper, we experimentally investigate the effects of the surface roughness of an object and the test detector's transverse size on the SNR and the resolution of RGI, which can also be confirmed by the analytical expression of the point spread function (PSF) and the SNR of the imaging system. Comparative studies on both rough objects and smooth objects also are performed. In both cases, an increase of the reflective angle will result in an enhancement of the SNR, although the results

indicate the smooth object is more easily affected by the angle. We believe our research could be very useful for remote sensing system applications.

This paper is organized into four sections. In Section 2, we present the experimental description and the theoretical considerations to obtain RGI with rough objects. Section 3 gives the related experimental results and discussion and conclusions are derived in Section 4.

## 2. EXPERIMENTAL DESCRIPTION AND THEORETICAL CONSIDERATIONS

Figure 1 presents the experimental setup for GI for a rough object. The pseudo-thermal light source, which is obtained by modulating a pulsed Nd:YAG laser with wavelength $\lambda$ into a slowly rotating ground glass, is divided by a 50%–50% nonpolarizing beam splitter (BS) into two beams (a test beam and a reference beam), which are described by their impulse response function $h_t(u_2, x_t)$ and $h_r(u_1, x_r)$, respectively. The light in the test beam travels through a diffuse-reflecting object and an objective lens with focal length $f$. Then all the randomly scattered and reflected photons from the surface of the object are collected by a bucket detector ($D_t$). The reference beam contains nothing but free-space propagation from the source to a CCD camera ($D_r$) with high spatial resolution, which is used to record the intensity distribution at $x_r$.

Using a correlator, all the information about the object can be constructed by measuring the correlation function between the intensity fluctuations [4],

$$G(x_r, x_t) = \left| \int \langle E^*(u_1)E(u_2)\rangle h_r(u_1, x_r)h_t^*(u_2, x_t)\mathrm{d}u_1\mathrm{d}u_2 \right|^2, \tag{1}$$

where $u_i$ $(i = 1, 2)$ represents the location of the source plane and $\langle E^*(u_1)E(u_2)\rangle$ is the first-order correlation function of the source.

Suppose the source with the desired Gaussian intensity distribution is fully spatially incoherent, then the first-order correlation function for the source can be written as

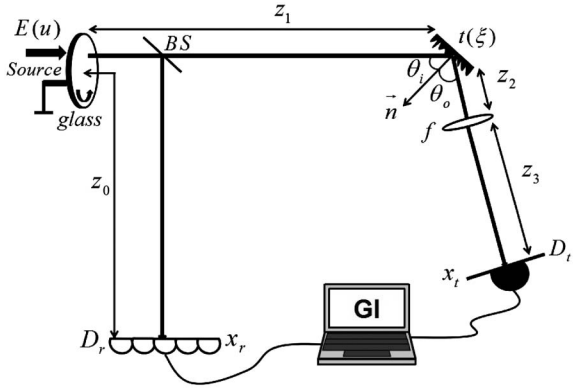


**Fig. 1.** Setup of reflective GI with the rough object. $\vec{n}$ denotes a unit vector pointing in the direction perpendicular to the object plane, and $x_r, x_t$ represent the coordinate at the reference detector plane and test detector plane, respectively.

$$\langle E^*(u_1)E(u_2)\rangle = \exp\left(-\frac{u_1^2 + u_2^2}{2a^2}\right)\delta(u_1 - u_2), \tag{2}$$

where $a$ is the transverse size of the source and $\delta(u)$ is the Dirac delta function.

In the reference arm, the detector $D_r$ is located at a distance $z_0$ from the source; thus, the impulse response function can be calculated by the Fresnel integral,

$$h_r(u_1, x_r) \propto \exp\left[-\frac{j\pi}{\lambda z_0}(x_r - u_1)^2\right]. \tag{3}$$

As for the test arm, an object with a rough surface is placed at a distance $z_1$ from the source, and the objective lens divides the distance between the object and the test detector into $z_2$ and $z_3$. Then, according to Ref. [25], the impulse response function for the object path is

$$h_t(u_2, x_t) \propto \int \mathrm{d}\xi R(\xi)\exp[j\phi(\xi)] \times \exp\left[-\frac{j\pi}{\lambda z_1}(\xi\cos\theta_i - u_2)^2\right] \times \exp\left[\frac{j\pi}{\lambda f}\left(1 - \frac{z_3}{z_2}\right)\xi^2\cos^2\theta_o - \frac{2j\pi}{\lambda f}\xi x_t\cos\theta_o\right], \tag{4}$$

where $\theta_i$ and $\theta_o$ respectively signify the incident angle and reflective angle. $R(\xi)$ represents the reflectivity of the object and $\phi(\xi)$ indicates the phase delay.

Substituting Eqs. (2)–(4) into Eq. (1) and using the related calculation methods in Ref. [29], the second-order correlation function can be simplified as

$$G(x_r, x_t) \propto \int \mathrm{d}\xi|R(\xi)|^2 \times \exp\left[-\frac{2\alpha(\beta_0 x_r - \beta_1\xi\cos\theta_i)^2}{\alpha^2 + (\beta_0 - \beta_1)^2}\right], \tag{5}$$

where $\alpha = \frac{1}{a^2}$, $\beta_0 = \frac{\pi}{\lambda z_0}$, and $\beta_1 = \frac{\pi}{\lambda z_1}$. The exponential function in the integral can be considered as the PSF of our imaging system, from which we can quantitatively derive that both the roughness of the object and the test detector's transverse size have no influence on imaging resolution.

If there is a detector with the effective transverse size $D$ in the test arm and there are $n$ shot measurements, then the SNR can be defined, according to Refs. [28,30], as

$$\mathrm{SNR} = \frac{G(x_r, x_t)}{\Delta G(x_r, x_t)} = \frac{\sqrt{n}}{[a^4\pi^2A^2/G^2(x_r) + 4\pi a^2 A/G(x_r) + 3]^{1/2}}, \tag{6}$$

$$G(x_r) \propto \int \mathrm{d}\xi\mathrm{d}\xi' R(\xi)R^*(\xi')\exp\{-\sigma_\phi^2[1 - e^{-(\xi-\xi')^2/l_c^2}]\} \times \exp\left\{-\frac{j\pi[z_1\cos^2\theta_o + (z_2 + z_3)\cos^2\theta_i](\xi^2 - \xi'^2)}{\lambda z_1(z_2 + z_3)}\right\} \times \mathrm{sinc}\left[\frac{a(\xi'\cos\theta_i - x_r)}{\lambda z_1}\right]\mathrm{sinc}\left[\frac{a(\xi\cos\theta_i - x_r)}{\lambda z_1}\right] \times \mathrm{sinc}\left[\frac{D\cos\theta_o(\xi - \xi')}{\lambda(z_2 + z_3)}\right], \tag{7}$$

and $A = \int d\xi d\xi' R(\xi) R^*(\xi') \exp\{-\sigma_\phi^2[1 - e^{-(\xi-\xi')^2/l_c^2}]\}$. $\sigma_\phi^2$ is the variance of phase, which reflects the variance of the surface height fluctuations and $l_c$ is the surface correlation length. Increasing the roughness of the object surface can reduce the value of $A$ and combining Eq. (6) with Eq. (7), it is not difficult to find that the SNR decreases with the increment of the surface roughness. Also, both the larger reflective angle and the smaller test detector size correspond to the higher SNR.

## 3. EXPERIMENTAL RESULTS

In our experiment, the focal length of the lens in the test arm is $f = 35$ mm, which is used to focus all the reflected and scattered photons onto the active area of the detector ($D_t$) with a transverse size $D$. The imaging object (a double slit) is made using sandpaper with different mesh numbers ($N$), which is covered by white reflective paint. Here we define the roughness of the object with the mesh number of the sandpaper. The smaller the mesh number is, the higher the roughness of the object. The double slit has a slit width of 0.5 mm and a center-to-center separation of 1 mm. The reference detector and the reflective object are placed at equal distances from the source, i.e., $z_0 = z_1 = 175$ mm. In addition, the incident angle shown in Fig. 1 is fixed at $\theta_i = \pi/4$, and other parameters are chosen as $z_2 = 35$ mm, $z_3 = 245$ mm, $\lambda = 532$ mm, and $a = 1$ mm.

First, we experimentally investigate the effect from the roughness of the object imaged on RGI (see Fig. 2). In our experiments, the reflective angle of the light source is set as $\theta_o = 0$ and the ghost image is reconstructed by second-order intensity correlation measurement under different mesh numbers $N$. To obtain a high-quality image, all the patterns are obtained with 10,000 realizations. As shown in Figs. 2(a)–2(c), we use $N = 240$, 360, and 600, which corresponds to very rough, slightly rough, and slightly smooth surfaces, respectively. The black solid lines in the lower section are the normalized horizontal sections of the experimental patterns in the upper areas. The SNRs from Figs. 2(a)–2(c) versus the mesh number is plotted in Fig. 2(d). One can see that a decrease of the surface roughness of the object results in an increase of SNR. At the same time, the horizontal section curves indicate that the imaging resolution remains unchanged, except that the background noise is weakened, which is in accordance with the analytical results given by Eqs. (5)–(7).

Next, let us consider the influence of the transverse size of the detector in the test arm by using the double slit with the same roughness ($N = 240$), as shown in Fig. 3. The incident and reflective angles are chosen as $\pi/4$. From Figs. 3(a)–3(c), the detector's transverse sizes $D$ are chosen as 2070, 690, and 172.5 μm, respectively. The other parameters in the experiment remain unchanged. Similarly, the relationship between SNR and the transverse size of the test detector is shown in Fig. 3(d). Obviously, with the increment of the transverse size $D$, the SNR becomes smaller. In other words, a small-sized detector is helpful to improve SNR. Moreover, the following black curves indicate that the resolution of images hardly depends on $D$, which can be well interpreted by Eq. (5) and also confirm the theoretical results depicted in Fig. 4 in Ref. [28].

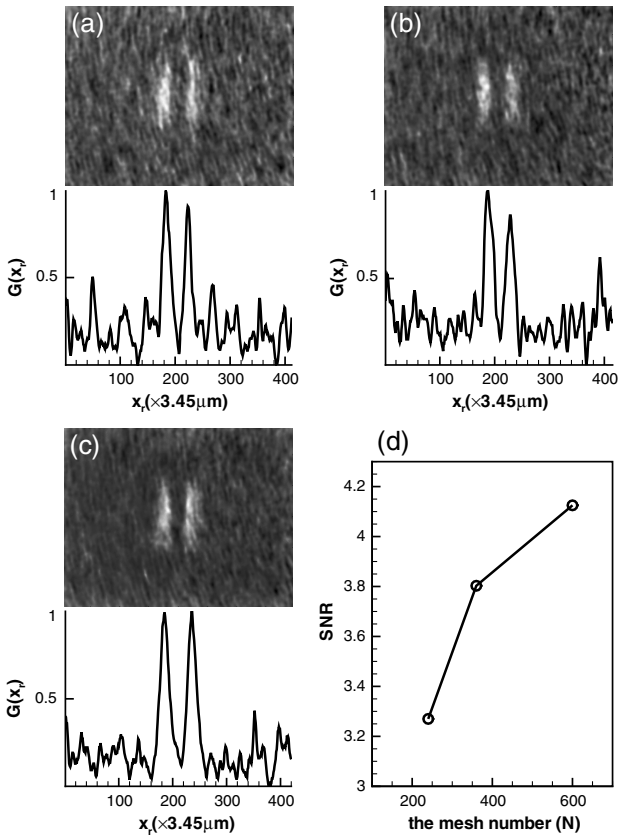


**Fig. 2.** Retrieved ghost images of the rough object with 10,000 measurements under different degrees of surface roughness. From (a) to (c), the value of mesh number $N$ is 240, 360, and 600, respectively. Black solid curves in the lower area show the normalized horizontal sections of the images. (d) Dependence of the corresponding SNR on the mesh number $N$. The incident angle is $\theta_i = \pi/4$, and the reflective angle is $\theta_o = 0$.

In Fig. 4, we comparatively study GI of rough and smooth objects based on different reflective angles ($\theta_o = \pi/4$ and $5\pi/12$). For the rough object, if we select the roughness represented by the mesh number $N = 240$ and the incident angle is still $\pi/4$, then the retrieved images are depicted in the Figs. 4(a) and 4(b), and the SNR values are 3.3542 and 3.5377, respectively. For a smooth object (a double strip, consisting of a rectangular silver mirror whose central part is blackened by a light-absorbing strip, are separated by 0.6 mm, and have a width 0.2 mm), other parameters of the experiment are the same as those of the rough object except for the absence of the lens. Because it is equivalent to specular reflection, the incident angle and the reflected angle are equal. Figures 4(c) and 4(d) show the images under the condition of $\theta_i = \theta_o$ being $\pi/4$ and $5\pi/12$, respectively. The corresponding values of SNR are 3.7286 and 4.4994. Obviously, the SNR of RGI can be improved to some extent with the increment of the reflective angle. Compared with the ghost image of rough surface, the result of the smooth surface corresponds to a better SNR. We also note that when the reflective angle increases, the image of the double slits with a smooth surface becomes thinner. For the rough object, the images are almost unchanged because the

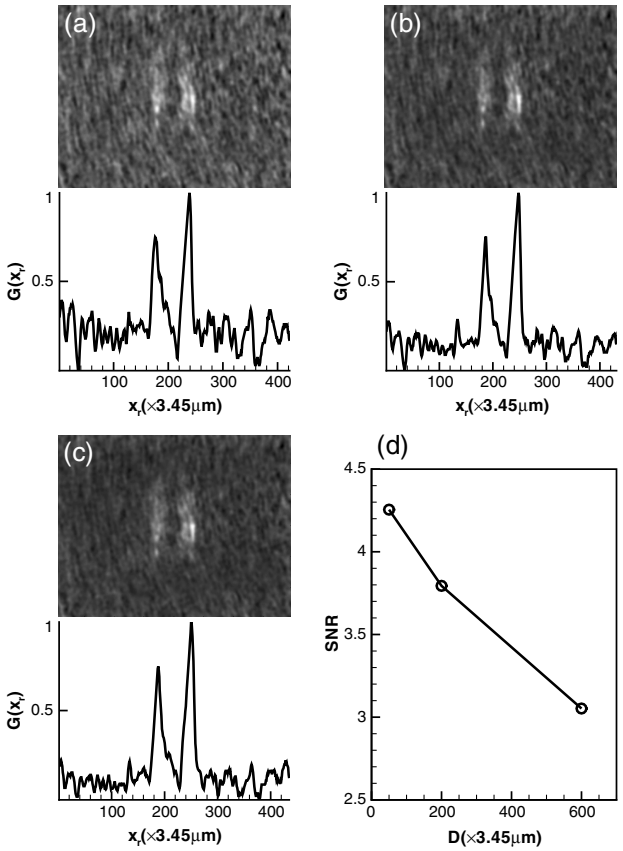


**Fig. 3.** Acquired images of the reflective target with a rough surface under different test detectors' transverse sizes $D$. In (a)–(c), the transverse sizes are 2070, 690, and 172.5 μm, respectively. (d) The corresponding SNR versus $D$. Other parameters are chosen as $N = 240$, and $\theta_i = \theta_o = \pi/4$.

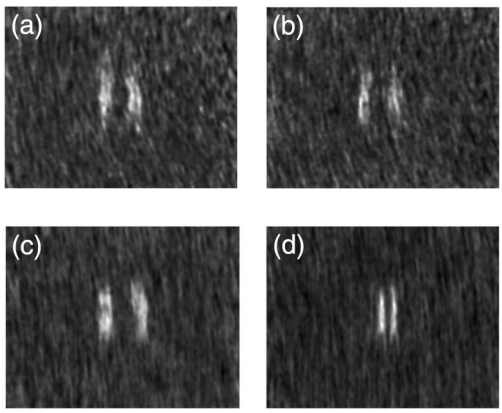


**Fig. 4.** Experimental results of GI for a rough object and a smooth target under different reflective angles $\theta_o$. (a) and (b) are ghost images of a rough object with $N = 240$, $\theta_i = \pi/4$, $\theta_o = \pi/4$, and $5\pi/12$, respectively. (c) and (d) are the results of a smooth target under $\theta_i = \theta_o = \pi/4$ and $5\pi/12$, respectively.

range of the smooth object illuminated by the light beam is decreased when the angle increases while the direction of photon propagation remains consistent. The size of image retrieved by specular reflection directly related to the number of photons detected by the test detector, while the surfaces of rough objects result in diffuse reflection and the photons are randomly scattered in all possible directions, so ghost images with the same size can be formed.

## 4. CONCLUSION

In conclusion, we have experimentally investigated RGI with different rough surfaces. Our experimental results clearly demonstrate that the SNR of patterns can be further enhanced using a reflective object with low roughness, a small-sized detector, and a large reflective angle. In addition, the roughness of the target and the transverse size of test detector were shown to have almost no influence on the resolution of RGI, which is in agreement with the corresponding theoretical results. Additionally, under the same conditions, although the SNRs of both rough and smooth objects increase with the increment of reflective angle, the latter is better than the former.

**Funding.** National Natural Science Foundation of China (NSFC) (61372102, 61571183); Natural Science Foundation of Hunan Province (2017JJ1014)

## REFERENCES

1. T. Pittman, Y. Shih, D. Strekalov, and A. Sergienko, "Optical imaging by means of two-photon quantum entanglement," Phys. Rev. A **52**, R3429–R3432 (1995).
2. D. Strekalov, A. Sergienko, D. Klyshko, and Y. H. Shih, "Observation of two-photon ghost interference and diffraction," Phys. Rev. Lett. **74**, 3600–3603 (1995).
3. R. S. Bennink, S. J. Bentley, and R. W. Boyd, "'Two-photon' coincidence imaging with a classical source," Phys. Rev. Lett. **89**, 113601 (2002).
4. J. Cheng and S. S. Han, "Incoherent coincidence imaging and its applicability in X-ray diffraction," Phys. Rev. Lett. **92**, 093903 (2004).
5. F. Ferri, D. Magatti, A. Gatti, M. Bache, E. Brambilla, and L. A. Lugiato, "High-resolution ghost image and ghost diffraction experiments with thermal light," Phys. Rev. Lett. **94**, 183602 (2005).
6. A. Valencia, G. Scarcelli, M. D'Angelo, and Y. Shih, "Two-photon imaging with thermal light," Phys. Rev. Lett. **94**, 063601 (2005).
7. C. Zhang, S. X. Guo, J. S. Cao, J. Guan, and F. L. Gao, "Object reconstitution using pseudo-inverse for ghost imaging," Opt. Express **22**, 30063–30073 (2014).
8. W. L. Gong, "High-resolution pseudo-inverse ghost imaging," Photon. Res. **3**, 234–237 (2015).
9. C. Q. Zhao, W. L. Gong, M. L. Chen, E. R. Li, H. Wang, W. D. Xu, and S. S. Han, "Ghost imaging lidar via sparsity constraints," Appl. Phys. Lett. **101**, 141123 (2012).
10. W. Yu, M. Li, and X. Yao, "Adaptive compressive ghost imaging based on wavelet trees and sparse representation," Opt. Express **22**, 7133–7144 (2014).
11. Y. Kang, Y. P. Yao, Z. H. Kang, L. Ma, and T. Y. Zhang, "Performance analysis of compressive ghost imaging based on different signal reconstruction techniques," J. Opt. Soc. Am. A **32**, 1063–1067 (2015).
12. Y. R. Huo, H. J. He, and F. Chen, "Compressive adaptive ghost imaging via sharing mechanism and fellow relationship," Appl. Opt. **55**, 3356–3367 (2016).
13. W. L. Gong, C. Q. Zhao, H. Yu, M. L. Chen, W. D. Xu, and S. S. Han, "Three-dimensional ghost imaging lidar via sparsity constraint," Sci. Rep. **6**, 26133 (2016).
14. W. Chen and X. D. Chen, "Ghost imaging for three-dimensional optical security," Appl. Phys. Lett. **103**, 221106 (2013).
15. H. Yu, E. R. Li, W. L. Gong, and S. S. Han, "Structured image reconstruction for three-dimensional ghost imaging lidar," Opt. Express **23**, 14541–14551 (2015).

16. X. Zeng, Y. F. Bai, X. H. Shi, Y. Gao, and X. Q. Fu, "The influence of the positive and negative defocusing on lensless ghost imaging," Opt. Commun. **382**, 415–420 (2016).
17. M. Bina, D. Magatti, M. Molteni, A. Gatti, L. A. Lugiato, and F. Ferri, "Backscattering differential ghost imaging in turbid media," Phys. Rev. Lett. **110**, 083901 (2013).
18. C. Yang, C. L. Wang, J. Guan, C. Zhang, S. X. Guo, W. L. Gong, and F. L. Gao, "Scalar-matrix-structured ghost imaging," Photon. Res. **4**, 281–285 (2016).
19. L. Wang and S. M. Zhao, "Fast reconstructed and high-quality ghost imaging with fast Walsh–Hadamard transform," Photon. Res. **4**, 240–244 (2016).
20. R. Meyers, K. S. Deacon, and Y. Shih, "Ghost-imaging experiment by measuring reflected photons," Phys. Rev. A **77**, 041801 (2008).
21. L. Basano and P. Ottonello, "Diffuse-reflection ghost imaging from a double-strip illuminated by pseudo-thermal light," Opt. Commun. **283**, 2657–2661 (2010).
22. N. S. Bisht, E. K. Sharma, and H. C. Kandpal, "Experimental observation of lensless ghost imaging by measuring reflected photons," Opt. Lasers Eng. **48**, 671–675 (2010).
23. N. D. Hardy and J. H. Shapiro, "Ghost imaging in reflection: resolution, contrast, and signal-to-noise ratio," Proc. SPIE **7815**, 78150L (2010).
24. N. D. Hardy and J. H. Shapiro, "Reflective ghost imaging through turbulence," Phys. Rev. A **84**, 063824 (2011).
25. C. F. Wang, D. W. Zhang, Y. F. Bai, and B. Chen, "Ghost imaging for a reflected object with a rough surface," Phys. Rev. A **82**, 063814 (2010).
26. C. Luo and J. Cheng, "Reflective ghost diffraction for objects with rough surfaces," J. Opt. Soc. Am. A **30**, 1166–1171 (2013).
27. D.-F. Shi, F. Wang, H. Jian, C. Kai-Fa, K. Yuan, H. Shun-Xing, and W. Ying-Jian, "Compressed polarimetric ghost imaging of different material's reflective objects," Opt. Rev. **22**, 882–887 (2015).
28. W. L. Gong, "Correlated imaging for a reflective target with a smooth or rough surface," J. Opt. **18**, 085702 (2016).
29. Y. Gao, Y. Bai, and X. Fu, "Point-spread function in ghost imaging system with thermal light," Opt. Express **24**, 25856–25866 (2016).
30. J. Cheng, S.-S. Han, and Y.-J. Yan, "Resolution and noise in ghost imaging with classical thermal light," Chin. Phys. **15**, 2002–2006 (2006).